The True Role of Accelerometer Feedback in Quadrotor Control

Philippe Martin, Erwan Salaun

The True Role of Accelerometer Feedback in Quadrotor Control

Philippe Martin and Erwan Salaün

***Abstract*— A revisited quadrotor model is proposed, including in particular the so-called rotor drag. It differs from the model usually considered, even at first order, and much better explains the role of accelerometer feedback in control algorithms. The theoretical derivation is supported by experimental data.**

I. Introduction

Quadrotor control has been an active area of investigation for several years. On the one hand the quadrotor has several qualities, among them its very simple mechanical design, and qualifies as a viable concept of mini Unmanned Aerial Vehicle (UAV) for real-life missions; on the other hand it is perceived in the control community as a very rich case study in theoretical and applied control. The first control objective is to ensure a stable flight at moderate velocities and in particular in hovering; this fundamental building block is then used to develop higher-level tasks.

But for experiments designed to work only in the lab with an off-board measuring device, e.g. [1], quadrotors all rely at the heart on strapdown MEMS inertial sensors (gyroscopes and accelerometers). These inertial sensors may be used alone (as far as horizontal stabilization is concerned) [2], or supplemented by other sensors which provide usually some position-related information. Representative designs are: ultrasonic rangers [3]; (simple) GPS module when outdoors and infrared rangers when indoors [4]; carrier phase differential GPS [5]; laser rangefinder [6]; vision system [7], [8], [9]; laser rangefinder and vision system [10]. Unfortunately those extra sensors have inherent drawbacks (low bandwidth, possible temporary unavailability, etc.), hence inertial sensors remain essential for basic stabilization.

Nearly all the papers in the literature rely on the same physical model: only aerodynamic forces and moments proportional to the square of the propellers angular velocities are explicitly taken into account. Other aerodynamics effects are omitted and considered as small unmodeled disturbances to be rejected by the control law. The alleged reason is that these effects are proportional to the square of the quadrotor linear velocity, hence very small near hovering. Few authors explicitly consider other aerodynamic effects: [11] considers aerodynamic stability derivatives, but draw no clear-cut conclusion about their importance; [12], [13] consider without physical motivation aerodynamic effects linear w.r.t. the quadrotor linear and angular velocities, but propose negligible numerical values; [5] judges them negligible at low velocities, and focus on nonlinear aspects at moderate velocities; [14] physically motivates the presence of effects nearly linear w.r.t the quadrotor linear and angular velocities, but provides no experimental data and is concerned only with the open-loop system.

Fig. 1. Our home-built quadrotor: the "Quadricopter".

On the other hand the vector $\vec{a}$ of accelerometer measurements can be used in two different ways (gyros are used in both cases; see II-C for more details about inertial sensors):

1) directly in the equation $\dot{\vec{V}} = \vec{g} + \vec{a}$ if extra sensors providing position or velocity information are available, thanks to a sensor fusion algorithm which estimates the velocity and the pitch and roll angles
2) through the approximation $\vec{a} \approx -\vec{g}$. Accordingly, the pitch and roll angles are estimated by a sensor fusion algorithm. Commercial "attitude sensors" such as the 3DM-GX[1] or the MTi[2] run exactly on this principle.

In both cases the sensor fusion algorithm can be an Extended Kalman Filter (EKF), a complementary filter, linear or nonlinear, or a nonlinear observer; see e.g. [15], [16] for an account of the two cases. Recall that MEMS inertial sensors are not accurate enough for "true" Schuler-based inertial navigation, see e.g. [17, chap. 5] for details.

Now, a puzzling issue arises: the "usual" physical model implies the longitudinal and lateral (in body axes) accelerometers should always measure zero, which clearly contradicts 2); as for 1), even if no particular form of the accelerometers measurements is assumed, one way wonder about the interest of using measurements known to be zero (and besides corrupted by noise and biases). Nevertheless many successful quadrotor flights have been reported, with control laws relying on 1) or 2) or even both, and there is no question that using accelerometers is beneficial.

This paper proposes a "revisited" model containing extra

Ph. Martin is with Centre Automatique et Systèmes, MINES ParisTech, Paris, France philippe.martin@mines-paristech.fr

E. Salaün is with the School of Aerospace Engineering, Georgia Institute of Technology, Atlanta, GA, USA erwan.salaun@gatech.edu

[1] www.microstrain.com

[2] www.xsens.com

aerodynamic terms proportional to the propeller angular velocity times the quadrotor linear or angular velocity. In particular the so-called rotor drag, though rather small, appears at first order and is essential to correctly account for the accelerometer measurements.

The paper runs as follows: the model is derived in II; its main features are experimentally validated in III; finally its implications on control schemes are discussed in IV.

II. Revisited quadrotor model

In this section we derive the linearized longitudinal subsystem (18)–(21) used in the rest of the paper. The reader not interested in the physical details can directly proceed to II-C.

A. Model of a single propeller near hovering

We first consider a single propeller rotating with angular velocity $\varepsilon_i\omega_i$ around its axis $\vec{k}_b$; ω_i is positive, with $\varepsilon_i = 1$ (resp. -1) for counterclockwise (resp. clockwise) rotation. The geometric center A_i of the propeller moves with a given velocity $\vec{V}_{A_i}$ while the rotor plane (by definition perpendicular to $\vec{k}_b$) undergoes angular velocity $\vec{\Omega}$; the total angular velocity of the propeller is thus $\vec{\Omega}+\varepsilon_i\omega_i\vec{k}_b$. Following e.g. [18, in particular chap. 5], the aerodynamic efforts on the propeller resolve into the force $\vec{F}_i$ and moment $\vec{M}_i$ at A_i,

$$\vec{F}_i = -a\omega_i^2\vec{k}_b - \omega_i\left(\lambda_1\vec{V}_{A_i}^{\perp} - \lambda_2\vec{\Omega}\times\vec{k}_b\right) + \varepsilon_i\omega_i\left(\lambda_3\vec{V}_{A_i}\times\vec{k}_b - \lambda_4\vec{\Omega}^{\perp}\right) \quad (1)$$

$$\vec{M}_i = -b\varepsilon_i\omega_i^2\vec{k}_b - \omega_i\left(\mu_1\vec{V}_{A_i}^{\perp} + \mu_2\vec{\Omega}\times\vec{k}_b\right) - \varepsilon_i\omega_i\left(\mu_3\vec{V}_{A_i}\times\vec{k}_b + \mu_4\vec{\Omega}^{\perp}\right), \quad (2)$$

where a, b, the λ_i's and μ_i's are positive constants; the projection of a vector $\vec{U}$ on the rotor plane is

$$\vec{U}^{\perp} := \vec{k}_b\times\left(\vec{U}\times\vec{k}_b\right) = \vec{U} - \left(\vec{U}\cdot\vec{k}_b\right)\vec{k}_b.$$

The above relations rely on classical blade element theory, with two extra simplifications, and (approximately) apply to any propeller, rigid or not:

- higher-order terms in linear and angular velocities have been neglected. This is valid near hovering, i.e. for small $\vec{V}_{A_i}$ and $\vec{\Omega}$. Here $\vec{V}_{A_i}$ "small" means small with respect to the propeller tip speed (about $40m/s$ in our case), so that $5m/s$ can be considered small
- linear and angular accelerations have been neglected. Their contribution is small since the mass of the propeller is in our case very small with respect to the total mass of the quadrotor.

The velocities in the previous equations are of course velocities with respect to the air stream, not with respect to the ground. They coincide when there is no wind, which we assume in the sequel.

The term $\omega_i\lambda_1\vec{V}_{A_i}^{\perp}$ in (1) is often called *H-force* or *rotor drag* in the helicopter literature. Also notice the simplified expressions (1)-(2), though directly based on textbook aerodynamics, do not seem to appear in the literature under this compact form very handy for control purposes.

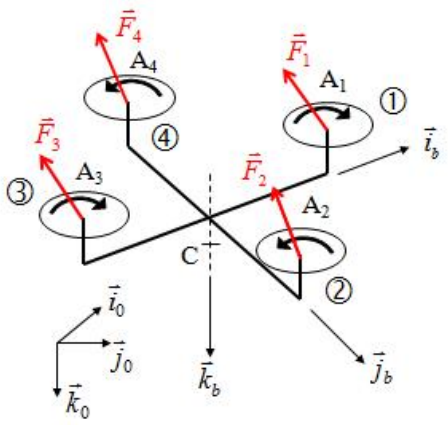

Fig. 2. Sketch of the complete quadrotor.

B. Model of the complete quadrotor

The quadrotor consists of a rigid frame with four propellers (directly) driven by electric motors, see fig. 2. The structure is symmetrically arranged, with one pair of facing propellers rotating clockwise and the other pair counterclockwise. The four propellers have the same axis $\vec{k}_b$; $\vec{\imath}_b := \frac{\vec{A_3A_1}}{\|\vec{A_3A_1}\|}$, $\vec{\jmath}_b := \frac{\vec{A_4A_2}}{\|\vec{A_4A_2}\|}$ and $\vec{k}_b$ then form a direct coordinate frame. Let A be the geometric center of the A_i's and $l := \frac{1}{2}\|\vec{A_3A_1}\| = \frac{1}{2}\|\vec{A_2A_4}\|$; clearly, $\sum_{i=1}^4\vec{AA}_i = 0$.

The whole system $\mathcal{B}$, with mass m and center of mass C, thus involves five rigid bodies: the frame/stators assembly $\mathcal{B}_0$ and the four propeller/motor assemblies $\mathcal{B}_i$; clearly, $\vec{CA} = h\vec{k}_b$ for some (signed) length h. Resolved in the $(\vec{\imath}_b, \vec{\jmath}_b, \vec{k}_b)$ frame, the velocity of C reads $\vec{V}_C = u\vec{\imath}_b + v\vec{\jmath}_b + w\vec{k}_b$ and the angular velocity of $\mathcal{B}_0$ reads $\vec{\Omega} = p\vec{\imath}_b + q\vec{\jmath}_b + r\vec{k}_b$.

We assume the only efforts acting on $\mathcal{B}$ are the weight and the aerodynamic efforts created by the propellers as described in the previous section. In particular we neglect the drag created by the frame, which is quadratic with respect to the velocity, hence small at low velocities. Newton's laws for the whole system then read

$$m\dot{\vec{V}}_C = m\vec{g} + \sum_{i=1}^4\vec{F}_i \quad (3)$$

$$\dot{\vec{\sigma}}_C^{\mathcal{B}} = \sum_{i=1}^4\vec{CA}_i\times\vec{F}_i + \vec{M}_i, \quad (4)$$

where $\vec{\sigma}_C^{\mathcal{B}} = \int_{\mathcal{B}}\vec{CM}\times\dot{\vec{CM}}d\mu(M)$ is the kinetic momentum of $\mathcal{B}$. For each $\mathcal{B}_i$, we can further write

$$\dot{\vec{\sigma}}_{A_i}^{\mathcal{B}_i}\cdot\vec{k}_b = \vec{M}_i\cdot\vec{k}_b + \varepsilon_i\Gamma_i, \quad (5)$$

where $\vec{\sigma}_{A_i}^{\mathcal{B}_i} = \int_{\mathcal{B}_i}\vec{A_iM}\times\dot{\vec{A_iM}}d\mu(M)$ is the kinetic momentum of $\mathcal{B}_i$, and Γ_i is the (positive) torque created by the motor. For simplicity we have considered A_i as the center of mass of $\mathcal{B}_i$ (in fact the two points are slightly apart). We also consider the Γ_i's as the control inputs (it is nevertheless easy to include the behavior of the electric motors both for modeling and control).

In hovering $\vec{V}_C$ and $\vec{\Omega}$, hence $\vec{V}_{A_i}$ are zero; from (1)–(4) this implies $a(\omega_1^2+\omega_2^2+\omega_3^2+\omega_4^2) = mg$ and $\omega_1^2-\omega_2^2+\omega_3^2-\omega_4^2 = \omega_1^2-\omega_3^2 = \omega_2^2-\omega_4^2 = 0$, hence $\omega_i = \bar{\omega} := \sqrt{\frac{mg}{4a}}$. As a consequence $\sum_{i=1}^4 \varepsilon_i\omega_i$, $\sum_{i=1}^4 \omega_i \vec{AA}_i$ and $\sum_{i=1}^4 \varepsilon_i\omega_i \vec{AA}_i$ also vanish in hovering. Neglecting in the right-handsides of (3)–(5) second-order terms made up from $\vec{\Omega}$, $\vec{V}_C$, $\sum_{i=1}^4 \varepsilon_i\omega_i$, $\sum_{i=1}^4 \omega_i \vec{AA}_i$ and $\sum_{i=1}^4 \varepsilon_i\omega_i \vec{AA}_i$, which is consistent with the first extra simplification in section II-A, (3)–(5) read

$$\begin{aligned} m\dot{\vec{V}}_C &= mg\vec{g} - a\left(\omega_1^2+\omega_2^2+\omega_3^2+\omega_4^2\right)\vec{k}_b \\ &\quad - \lambda_1(\omega_1+\omega_2+\omega_3+\omega_4)\vec{V}_C^{\perp} \qquad (6) \\ \dot{\vec{\sigma}}_C^{\mathcal{B}} &= -al(\omega_2^2-\omega_4^2)\vec{\imath}_b + al(\omega_1^2-\omega_3^2)\vec{\jmath}_b \\ &\quad - \varepsilon_1 b\left(\omega_1^2-\omega_2^2+\omega_3^2-\omega_4^2\right)\vec{k}_b \\ &\quad - (\omega_1+\omega_2+\omega_3+\omega_4)\left(\mu_1'\vec{V}_C\times\vec{k}_b + \mu_2''\vec{\Omega}^{\perp}\right) \\ &\quad - (\omega_1+\omega_2+\omega_3+\omega_4)\lambda_1 l^2 r\vec{k}_b \qquad (7) \\ \dot{\vec{\sigma}}_{A_i}^{\mathcal{B}_i}\cdot\vec{k}_b &= \varepsilon_i(\Gamma_i - b\omega_i^2), \qquad i=1,2,3,4. \qquad (8) \end{aligned}$$

Indeed,

$$\begin{aligned} &\lambda_3\vec{V}_{A_i}\times\vec{k}_b - \lambda_4\vec{\Omega}^{\perp} \\ &\quad = \lambda_3\big(\vec{V}_C + C\dot{\vec{A}} + A\dot{\vec{A}}_i\big)\times\vec{k}_b - \lambda_4\vec{\Omega}^{\perp} \\ &\quad = \lambda_3\left(\vec{V}_C + h\vec{\Omega}\times\vec{k}_b + \vec{\Omega}\times\vec{AA}_i\right)\times\vec{k}_b - \lambda_4\vec{\Omega}^{\perp} \\ &\quad = \lambda_3\vec{V}_C\times\vec{k}_b + \lambda_4'\vec{\Omega}^{\perp} + r\lambda_3\vec{AA}_i \\ &\lambda_1\vec{V}_{A_i}^{\perp} - \lambda_2\vec{\Omega}\times\vec{k}_b \\ &\quad = \lambda_1\left(\vec{V}_C^{\perp} + \big(h\vec{\Omega}\times\vec{k}_b\big)^{\perp} + \big(\vec{\Omega}\times\vec{AA}_i\big)^{\perp}\right) - \lambda_2\vec{\Omega}\times\vec{k}_b \\ &\quad = \lambda_1\vec{V}_C^{\perp} - \lambda_2'\vec{\Omega}\times\vec{k}_b - r\lambda_1\vec{AA}_i\times\vec{k}_b, \end{aligned}$$

where we used the fact that $\vec{AA}_i$ is colinear to either $\vec{\imath}_b$ or $\vec{\jmath}_b$, and set $\lambda_2' =: \lambda_2 - h\lambda_1$ and $\lambda_4' := \lambda_4 + h\lambda_3$. Therefore,

$$\begin{aligned} \sum_{i=1}^4 \vec{F}_i &= -a\left(\sum_{i=1}^4\omega_i^2\right)\vec{k}_b - \left(\sum_{i=1}^4\omega_i\right)\left(\lambda_1\vec{V}_C^{\perp} - \lambda_2'\vec{\Omega}\times\vec{k}_b\right) \\ &\quad + \left(\sum_{i=1}^4\varepsilon_i\omega_i\right)\left(\lambda_3\vec{V}_C\times\vec{k}_b - \lambda_4'\vec{\Omega}^{\perp}\right) \\ &\quad + r\lambda_1\left(\sum_{i=1}^4\omega_i\vec{AA}_i\right)\times\vec{k}_b + r\lambda_3\left(\sum_{i=1}^4\varepsilon_i\omega_i\vec{AA}_i\right) \\ &\approx -a\left(\sum_{i=1}^4\omega_i^2\right)\vec{k}_b - \left(\sum_{i=1}^4\omega_i\right)\left(\lambda_1\vec{V}_C^{\perp} - \lambda_2'\vec{\Omega}\times\vec{k}_b\right), \end{aligned}$$

neglecting velocity second order terms in the last line. A further simplification, valid for a rather rigid propeller, is to consider that λ_2' is zero. Indeed h is by design small, and for a rather rigid propeller so is λ_2. This yields

$$\sum_{i=1}^4 \vec{F}_i \approx -a\left(\sum_{i=1}^4\omega_i^2\right)\vec{k}_b - \lambda_1\left(\sum_{i=1}^4\omega_i\right)\vec{V}_C^{\perp}.$$

Similar computations yield

$$\begin{aligned} &\sum_{i=1}^4 C\vec{A}\times\vec{F}_i + \vec{AA}_i\times\vec{F}_i + \vec{M}_i \\ &\approx -a\left(\sum_{i=1}^4\omega_i^2\vec{AA}_i\right)\times\vec{k}_b - b\left(\sum_{i=1}^4\varepsilon_i\omega_i^2\right)\vec{k}_b \\ &\quad - r\lambda_1 l^2\left(\sum_{i=1}^4\omega_i\right)\vec{k}_b - \left(\sum_{i=1}^4\omega_i\right)\left(\mu_1'\vec{V}_C\times\vec{k}_b + \mu_2''\vec{\Omega}^{\perp}\right), \end{aligned}$$

where $\mu_1' := \mu_1 - h\lambda_1$, $\mu_2' := \mu_2 - h\mu_1$ and $\mu_2'' := \mu_2' - h\lambda_2$.

We then evaluate the left-handsides of (6)–(8). Since the approach is fairly standard we just give the final result,

$$\begin{pmatrix} \dot{\vec{V}}_C\cdot\vec{\imath}_b \\ \dot{\vec{V}}_C\cdot\vec{\jmath}_b \\ \dot{\vec{V}}_C\cdot\vec{k}_b \end{pmatrix} = \begin{pmatrix} \dot{u}+qw-rv \\ \dot{v}+ru-pw \\ \dot{w}+pv-qu \end{pmatrix} \qquad (9)$$

$$\begin{pmatrix} \dot{\vec{\sigma}}_C^{\mathcal{B}}\cdot\vec{\imath}_b \\ \dot{\vec{\sigma}}_C^{\mathcal{B}}\cdot\vec{\jmath}_b \\ \dot{\vec{\sigma}}_C^{\mathcal{B}}\cdot\vec{k}_b \end{pmatrix} = \begin{pmatrix} I\dot{p} + (J-I)qr + J_r q\sum_{i=1}^4\varepsilon_i\omega_i \\ I\dot{q} - (J-I)pr - J_r p\sum_{i=1}^4\varepsilon_i\omega_i \\ J\dot{r} + J_r\sum_{i=1}^4\varepsilon_i\dot{\omega}_i \end{pmatrix} \qquad (10)$$

$$\dot{\vec{\sigma}}_{A_i}^{\mathcal{B}_i}\cdot\vec{k}_b = J_r(\dot{r}+\varepsilon_i\dot{\omega}_i), \qquad i=1,2,3,4, \qquad (11)$$

where I, J, I_r, J_r are strictly positive constants. Notice we replaced in the computation of the inertia tensors the actual propellers by disks with the same masses and radii, and took advantage of the various symmetries; this "averaging" approximation is justified by the fact that the propeller angles vary much faster than all the other kinematic variables (besides this approximation is already heavily used in the blade element theory used to derive (1)-(2)).

To describe the orientation of the quadrotor we use the classical ϕ, θ, ψ Euler angles (quaternions could of course be used). The direction cosine matrix $R_{\phi,\theta,\psi}$ to go from Earth coordinates to aircraft coordinates is then

$$\begin{pmatrix} C\theta C\psi & C\theta S\psi & -S\theta \\ S\phi S\theta C\psi - C\phi S\psi & S\phi S\theta S\psi + C\phi C\psi & S\phi C\theta \\ C\phi S\theta C\psi + S\phi S\psi & C\phi S\theta S\psi - S\phi S\psi & C\phi C\theta \end{pmatrix},$$

so that $\vec{g} = g(-\vec{\imath}_b\sin\theta + \vec{\jmath}_b\sin\phi\cos\theta + \vec{k}_b\cos\phi\cos\theta)$.

Finally the angles and angular velocities are linked by

$$\dot{\phi} = p + (q\sin\phi + r\cos\phi)\tan\theta \qquad (12)$$

$$\dot{\theta} = q\cos\phi - r\sin\phi \qquad (13)$$

$$\dot{\psi} = \frac{q\sin\phi + r\cos\phi}{\cos\theta}. \qquad (14)$$

Equations (6)–(14) form the complete 13-dimensional quadrotor model.

C. Model of the inertial sensors

The quadrotor is equipped with strapdown triaxial gyroscope and accelerometer. Without restriction, we assume the sensing axes coincide with $\vec{\imath}_b, \vec{\jmath}_b, \vec{k}_b$. The gyroscope measures the angular velocity $\vec{\Omega}$, projected on its sensing axes, i.e. $(g_x, g_y, g_z) := (p, q, r)$; the accelerometer measures the specific acceleration $\vec{a} := \dot{\vec{V}}_P - \vec{g}$ of the point P where it is

located, projected on its sensing axe; see e.g. [17, chap. 4] for details on inertial sensors. Hence by (3) if the accelerometer is located at the center of mass C, which is the case for most quadrotors, it measures $\vec{a} = \dot{\vec{V}}_C - \vec{g} = \frac{1}{m}\sum_{i=1}^{4} \vec{F}_i$; by (6) the accelerometer thus measures

$$a_x := \vec{a} \cdot \vec{\imath}_b \qquad \approx -\frac{\lambda_1}{m}(\omega_1 + \omega_2 + \omega_3 + \omega_4)u \tag{15}$$

$$a_y := \vec{a} \cdot \vec{\jmath}_b \qquad \approx -\frac{\lambda_1}{m}(\omega_1 + \omega_2 + \omega_3 + \omega_4)v \tag{16}$$

$$a_z := \vec{a} \cdot \vec{k}_b \qquad \approx -\frac{a}{m}\left(\omega_1^2 + \omega_2^2 + \omega_3^2 + \omega_4^2\right). \tag{17}$$

D. Linearized model

To highlight the salient features of the revisited model (6)–(14), it is enough to consider its first-order approximation. Suitably putting together variables, this linearized model splits into four independent subsystems:

- longitudinal subsystem (input $\Gamma_1 - \Gamma_3$)

$$\begin{aligned} m\dot{u} &\approx -mg\theta - 4\lambda_1\bar{\omega}u \\ \dot{\theta} &\approx q \\ I\dot{q} &\approx 4\mu_1'\bar{\omega}u - 4\mu_2''\bar{\omega}q + 2al\bar{\omega}(\omega_1 - \omega_3) \\ J_r(\dot{\omega}_1 - \dot{\omega}_3) &\approx \Gamma_1 - \Gamma_3 - 2b\bar{\omega}(\omega_1 - \omega_3). \end{aligned}$$

  From II-C, $a_x \approx -\frac{4\lambda_1\bar{\omega}}{m}u$ and $g_y = q$ are measured
- lateral subsystem (input $\Gamma_4 - \Gamma_2$, states $v, \phi, p, \omega_4 - \omega_2$)
- vertical subsystem (input $\sum_{i=1}^{4}\Gamma_i$, states $w, \sum_{i=1}^{4}\omega_i$)
- heading subsystem (input $\sum_{i=1}^{4}\varepsilon_i\Gamma_i$, states $\psi, r, \sum_{i=1}^{4}\varepsilon_i\omega_i$).

We will concentrate on the longitudinal system, hence need not detail the other subsystems. Notice the longitudinal and lateral subsystems are the same up to a sign-reversing coordinate change. Setting $\omega_q := \omega_1 - \omega_3$, $\Gamma_q := \frac{\Gamma_1 - \Gamma_3}{J_r}$ and

$$(f_1, f_2, f_3, f_4, f_5) := \left(\frac{4\lambda_1\bar{\omega}}{m}, \frac{4\mu_1'\bar{\omega}}{I}, \frac{4\mu_2''\bar{\omega}}{I}, \frac{2al\bar{\omega}}{I}, \frac{2b\bar{\omega}}{J_r}\right),$$

the longitudinal subsystem reads

$$\dot{u} = -f_1 u - g\theta \tag{18}$$

$$\dot{\theta} = q \tag{19}$$

$$\dot{q} = f_2 u - f_3 q + f_4\omega_q \tag{20}$$

$$\dot{\omega}_q = \Gamma_q - f_5\omega_q, \tag{21}$$

with measurements $a_x = -f_1 u$ and $g_y = q$.

E. Departure from literature

Most authors consider a propeller model with only the $\vec{k}_b$ terms in (1)-(2), i.e. with all λ_i's and μ_i's equal to zero. They thus end up with the quadrotor model

$$m\dot{\vec{V}}_C = m\vec{g} - a\left(\omega_1^2 + \omega_2^2 + \omega_3^2 + \omega_4^2\right)\vec{k}_b \tag{22}$$

$$\begin{aligned} \dot{\vec{\sigma}}_C = &-b\varepsilon_1\left(\omega_1^2 - \omega_2^2 + \omega_3^2 - \omega_4^2\right)\vec{k}_b \\ &+ al(\omega_1^2 - \omega_3^2)\vec{\jmath}_b - al(\omega_2^2 - \omega_4^2)\vec{\imath}_b. \end{aligned} \tag{23}$$

There is obviously a problem with such a model: indeed $\vec{a} = \dot{\vec{V}}_C - \vec{g}$ is colinear with $\vec{k}_b$, hence $a_x = a_y = 0$, which is certainly not thought to be true! This paradox is usually not acknowledged, and the approximation $\vec{a} \approx -\vec{g}$ is used instead, i.e.

$$(a_x, a_y, a_z) \approx (g\sin\theta, -g\sin\phi\cos\theta, -g\cos\phi\cos\theta). \tag{24}$$

The alleged motivation is that $\dot{\vec{V}}_C$ is small near hovering, at least in the mean. This is indeed true if the aircraft is stabilized by some extraneous means, but a very questionable assumption to use in a closed-loop perspective. Nevertheless, many successful flights with controllers relying on this approximation have been reported. We suggest in IV-C an explanation reconciling all those facts in the light of the revisited quadrotor model.

The longitudinal subsystem usually considered is then

$$\dot{u} = -g\theta \tag{25}$$

$$\dot{\theta} = q \tag{26}$$

$$\dot{q} = f_4\omega_q \tag{27}$$

$$\dot{\omega}_q = \Gamma_q - f_5\omega_q, \tag{28}$$

with measurements $a_x = g\theta$ and $g_y = q$, to be compared with (18)–(21) with measurements $a_x = -f_1 u$ and $g_y = q$.

III. Experimental validation

A. Experimental setup

To validate the model, we recorded flight data with our home-built "Quadricopter", see fig. 1. Due to limitations of our experimental setup, we could collect data to validate only the force model (18), but not the moment model (20); this is nevertheless the most important part of the model since it accounts for the accelerometer measurements. The quadrotor was fitted with a MIDG2 "GPS-aided Inertial Navigation System"[3] and a radio data link towards the ground station. The MIDG2 consists of a triaxial accelerometer, a triaxial gyroscope, a triaxial magnetometer, a GPS engine and an on-board computer. The raw measurements are fused by an EKF on the onboard computer to provide estimates of the orientation and of the velocity vector in Earth axes. The MIDG2 is an "independent" device with no knowledge of the specific system it is fitted on; it heavily relies on the GPS engine for good dynamic estimates, without using assumption (24). All the data can be issued at a pace up to 20ms. Due to the low throughput of the radio data link, only the accelerometer raw measurements a_{xm}, a_{ym} and the MIDG2-computed quantities ϕ_m, θ_m, ψ_m and V_x, V_y, V_z were transmitted to the ground station, at the reduced pace of 40ms.

We flew the quadrotor in repeated back and forth translations at a (nearly) constant altitude and recorded one minute of flight data. Since a GPS module is used the test was conducted outdoors, on a very calm day to respect the no-wind assumption.

B. Validation of the force model

Due to an imperfect mechanical design of our quadrotor, the MIDG2 case is not exactly aligned with the quadrotor

[3] www.microboticsinc.com

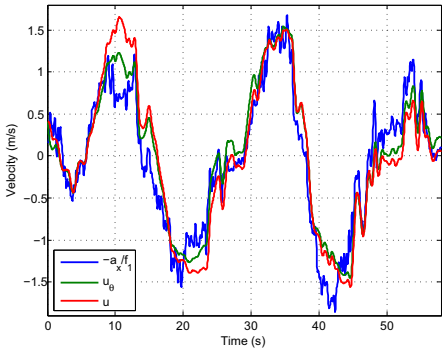

Fig. 3. Comparison between $-\frac{a_x}{f_1}$, u_θ and u.

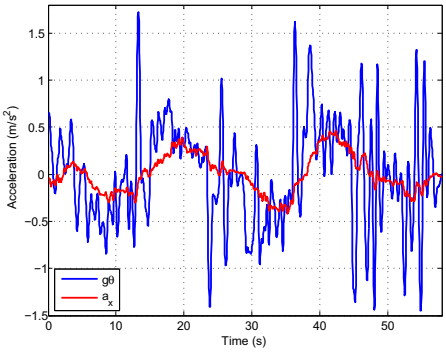

Fig. 4. Comparison between a_x and $g\theta$.

frame, but tilted by the unknown (small) angles ϕ_0, θ_0, ψ_0. The angle and acceleration data must be rotated accordingly to be expressed in the quadrotor axes (the velocity data need not correction, since expressed in Earth axes), that is

$$(\phi, \theta, \psi) = (\phi_m - \phi_0, \theta_m - \theta_0, \psi_m - \psi_0)$$
$$\begin{pmatrix} a_x \\ a_y \\ a_z \end{pmatrix} = R^T_{\phi_0,\theta_0,\psi_0} \begin{pmatrix} a_{xm} \\ a_{ym} \\ a_{zm} \end{pmatrix}.$$

Dropping higher-order terms, this yields

$$\begin{aligned} a_x &\approx a_{xm} - \psi_0 a_{ym} + \theta_0 a_{zm} &&\approx a_{xm} - \theta_0 g \\ a_y &\approx \psi_0 a_{xm} + a_{ym} - \phi_0 a_{zm} &&\approx a_{ym} + \phi_0 g. \end{aligned}$$

The velocity vector in body axes is obtained by

$$\begin{pmatrix} u \\ v \\ w \end{pmatrix} = R_{\phi,\theta,\psi} \begin{pmatrix} V_x \\ V_y \\ V_z \end{pmatrix},$$

and is considered as the "true" reference velocity to validate our modeling assumptions.

We also want to compute the velocities u_θ and v_ϕ predicted by the integration of the linearized force model (18)

$$\begin{aligned} \dot{u}_\theta &= -f_1 u_\theta - g\theta \\ \dot{v}_\phi &= -f_1 v_\phi + g\phi, \end{aligned}$$

with initial conditions $u_\theta(0) := u(0)$ and $v_\phi(0) := v(0)$.

The task was then to adjust $f_1, \phi_0, \theta_0, \psi_0$ to get a good fit between $-\frac{a_x}{f_1}$, u and u_θ on the one hand; and between $-\frac{a_y}{f_1}$, v and v_ϕ on the other hand. Since the accelerometer data are quite noisy and need some filtering, the same filter (5^{th}-order Bessel filter with 2Hz cutoff frequency) was applied to all the data to preserve the transfer functions among them.

With $(f_1, \phi_0, \theta_0, \psi_0) := (0.25\text{s}^{-1}, 1.2°, -2.4°, 2°)$ the agreement is good between the "true" (i.e. MIDG2-given) velocity u, the "accelerometer-based" velocity $-\frac{a_x}{f_1}$, and the velocity u_θ "predicted" by the model from the "true" (i.e. MIDG2-given) pitch angle, see fig. 3, which reasonably validates our force model. The agreement between $v, -\frac{a_y}{f_1}$ and v_ϕ, not shown for lack of space is equally good.

To test the traditional approximation (24) we also plotted $(a_x, g\theta)$, see fig. 4. Though the trend is roughly correct, the fit is much worse; the result is similar for $(a_y, -g\phi)$.

IV. Implications on control schemes

We now investigate the relevance of the revisited model in the presence of a feedback controller, with (section IV-A) and without (sections IV-B and IV-C) velocity measurements. We use the numerical values

$$(f_1, f_2, f_3, f_4, f_5) = (0.25, 0.76, -9.8, 0.34, 12.74);$$

f_1 was determined from flight tests, and f_4, f_5 from static tests on the motor-propeller subsystems. The aerodynamic coefficients f_2, f_3 were analytically derived; their values are plausible but nevertheless questionable.

A. Two-time-scale "full-state" feedback

We first assume the whole state is known, or which turns out to be equivalent, that u and q are measured without noise so that they can be used in ideal Proportional-Derivative (PD) controllers. It is customary to design a two-time-scale control law, with a fast inner loop to control q, ω_q and a slow outer loop to control u, θ.

The fast inner loop is the ideal PD controller

$$\Gamma_q = -\frac{k_p}{\varepsilon^2} q - \frac{k_d}{\varepsilon} \dot{q} + \frac{k_p}{\varepsilon^2} q_r,$$

where q_r is the desired pitch rate; k_p, k_d are the PD gains and $\varepsilon > 0$ is a "small" parameter. Applying this feedback to (18)-(21) yields

$$\begin{aligned} \dot{u} &= -f_1 u - g\theta \\ \dot{\theta} &= q \\ \varepsilon \dot{q} &= f_4 \tilde{\omega}_q + \mathcal{O}(\varepsilon) \\ \varepsilon \dot{\tilde{\omega}}_q &= -k_p q - f_4 k_d \tilde{\omega}_q + k_p q_r + \mathcal{O}(\varepsilon), \end{aligned}$$

where $\tilde{\omega}_q := \varepsilon \omega_q$. From standard arguments of singular perturbations theory [19], the convergence of the fast variables is up to order ε ruled by the well-known coefficient f_4 and the PD gains; and the behavior of the slow variables u, θ is up to order ε ruled by the slow approximation

$$\dot{u} = -f_1 u - g\theta \tag{29}$$
$$\dot{\theta} = q_r. \tag{30}$$

Hence the role of the aerodynamic coefficients f_2, f_3 is marginal if the inner loop is fast enough.

The slow outer loop is the ideal PD controller

$$q_r = k_1 u + k_2 \dot{u} - k_1 u_r,$$

where u_r is the desired velocity, and k_1, k_2 the PD gains. Applying this feedback to (29)-(30) yields

$$\begin{aligned}\dot{u} &= -f_1 u - g\theta \\ \dot{\theta} &= (k_1 - f_1 k_2)u - g k_2 \theta - k_1 u_r,\end{aligned}$$

with characteristic polynomial $s^2 + (f_1 + g k_2)s + g k_1$. A reasonable closed-loop settling time is about $1s$, which requires $g k_1 = 6^2$ and $f_1 + g k_2 = 6\sqrt{2}$. This means $f_1 = 0.25$ is negligible w.r.t to the effect of the controller.

We thus see that the revisited moment model (20) does not rely matter if the gyroscope measurements are good enough for a fast loop, which is usually the case in practice; nevertheless taking into account f_2 and especially f_3 may help to design a better inner loop. As for the force model (18), it does not really matter either, provided a velocity measurement is available, wich agrees with [5]. The importance of f_1 is nevertheless paramount to account for the accelerometer measurements, as will be seen in the following sections.

B. Usual interpretation of accelerometer feedback

Once the inner loop closed, the usual slow model is

$$\begin{aligned}\dot{u} &= -g\theta \\ \dot{\theta} &= q_r,\end{aligned}$$

with measurement $a_x = g\theta$. Since the velocity u is clearly not observable, the role of the outer loop is simply to control the measured angle θ. In theory the simple proportional feedback $q_r = k(\theta_r - \frac{a_x}{g})$ does the trick, but in practice the accelerometer measurements are too noisy to be directly used (not only because of the intrinsic sensor noise, but also because of mechanical vibrations). Instead an "angle estimator" is often used, based on the model $\dot{\theta} = q$ with measurements $a_x = g\theta$ and $g_y = q$. A more elaborate estimator, e.g. an EKF or a nonlinear observer, can also be used, see the references in the introduction; it is then based on the nonlinear kinematic equations (12)–(14), and relies on the approximation (24). Whatever the filter, the first-order approximation is essentially the linear observer $\dot{\hat{\theta}} = g_y + l(\frac{a_x}{g} - \hat{\theta})$; it can also be seen as a complementary filter since its transfer function is $\hat{\theta} = \frac{s}{s+l}\theta_q + \frac{l}{s+l}\theta_{a_x}$, where $\theta_q := \frac{q}{s}$ is the pitch angle obtained from gyro integration and $\theta_{a_x} := \frac{a_x}{g}$ the pitch angle given by the accelero.

The outer loop thus is the controller-observer

$$q_r = k(\theta_r - \hat{\theta}) \tag{31}$$

$$\dot{\hat{\theta}} = q + l\Big(\frac{a_x}{g} - \hat{\theta}\Big). \tag{32}$$

Applied to the usual model and defining the observation error $e_\theta := \hat{\theta} - \theta$, it yields the closed-loop system

$$\begin{aligned}\dot{u} &= -g\theta \\ \dot{\theta} &= k(\theta_r - \theta - e_\theta) \\ \dot{e}_\theta &= -l e_\theta.\end{aligned}$$

For θ_r constant, the last two equations have the unique steady state $(\theta, e_\theta) = (\theta_r, 0)$. The characteristic polynomial is

$$\Delta_0 := (s + k)(s + l),$$

and the closed-loop transfer functions are

$$\theta = \frac{k}{s+k}\theta_r \tag{33}$$

$$u = \frac{-gk}{s(s+k)}\theta_r. \tag{34}$$

Provided $k, l > 0$ we have as desired $(\theta, e_\theta) \to (\theta_r, 0)$, while u grows linearly unbounded. A good tuning of (31)-(32) requires for robustness that the controller and observer act in distinct time scales (Loop Transfer Recovery), i.e. $k \gg l$ or $l \gg k$. We consider in the sequel a "slow" observer, which is representative of commercial "angle sensors" such as the 3DM-GX, and a "fast" controller; for a settling time of about $1s$, we choose e.g. $k := \frac{1}{0.3}$ and $l := \frac{1}{12}$.

We tested this control scheme experimentally, with a rather satisfying result: the angle θ reaches the desired θ_r, though the dynamics is somewhat more sluggish than expected. The usual analysis could thus be considered as reasonably justified. Nevertheless it does not account for the following experimental observations already visible to the naked eye:

- when pushed away from hovering, the quadrotor returns to hovering (of course at a different position)
- when flying at a constant velocity u, the angle θ is not zero but approximately proportional to u
- in response to a constant θ_r, u does not grow unbounded but reaches a value approximately proportional to θ_r.

Though these experimental facts are well-known to people in the field, they do not seem to be reported in the literature. The discrepancy is usually attributed to the neglected second-order aerodynamical drag and the inevitably unperfect experimental conditions. Another more subtle discrepancy is that the observer gain l must be smaller than predicted by the theory to avoid a badly damped transient (e.g. $l = 1/3$ does not work well in practice).

As will be seen in the following section, these experimental facts can be explained by the revisited model.

C. Revisited interpretation of accelerometer feedback

We now apply the controller-observer (31)-(32) to the revisited longitudinal model. The closed-loop system is now

$$\begin{aligned}\dot{u} &= -f_1 u - g\theta \\ \dot{\theta} &= k(\theta_r - \theta - e_\theta) \\ \dot{e}_\theta &= -l\Big(\frac{f_1}{g}u + \theta + e_\theta\Big),\end{aligned}$$

with $e_\theta := \hat{\theta} - \theta$. For θ_r constant, the only steady state is $(u, \theta, e_\theta) = (-\frac{g}{f_1}\theta_r, \theta_r, 0)$; the characteristic polynomial is

$$\Delta = s^3 + (k + l + f_1)s^2 + f_1(k + l)s + f_1 k l.$$

If $k \gg l$, $\Delta \simeq (s + k)(s^2 + f_1 s + f_1 l)$, so that the closed-loop system is stable as soon as $k, l > 0$. Hence $\theta \to \theta_r$ as desired, and $e_\theta \to 0$ as expected from the observer; u now

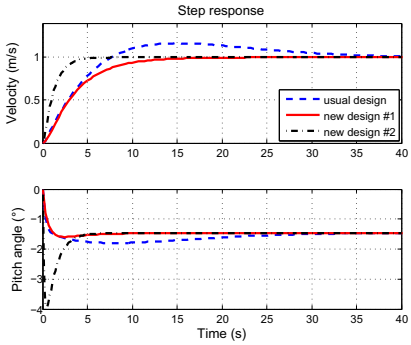

Fig. 5. Comparison between control schemes (simulation).

tends to the finite value $-\frac{g}{f_1}\theta_r$, which is more consistent with experimental tests. If moreover $l \ll f_1$,

$$\Delta \approx (s+f_1)(s+k)(s+l) = (s+f_1)\Delta_0.$$

As a consequence, the closed-loop transfer functions are

$$\begin{aligned} \theta &= \frac{k(s+f_1)(s+l)}{\Delta}\theta_r \qquad &&\approx \frac{k}{s+k}\theta_r \\ u &= \frac{-gk(s+l)}{\Delta}\theta_r \qquad &&\approx \frac{-gk}{(s+f_1)(s+k)}\theta_r, \end{aligned}$$

to be compared with (33)-(34): the angle dynamics is nearly the same as the one given by the usual interpretation, while the velocity dynamics is dominated by the rotor drag time constant $\frac{1}{f_1}$. Defining the reference velocity $u_r := -\frac{g}{f_1}\theta_r$, we see the usual control scheme, designed as an angle controller, is in fact a velocity controller!

The behavior experienced in practice is qualitatively and quantitatively well predicted by the revisited model, see fig. 5 ("usual design") the time response to a $-1.5°$ step in θ_r (i.e. a $1m/s$ step in u_r).

From this analysis, we see the importance of the coefficient f_1 is paramount: the usual scheme works reasonably well only because f_1 is positive and not too small.

D. A better control law

The performance of the usual control scheme is limited by the rotor drag time constant $\frac{1}{f_1}$. Better performance can be achieved by considering a controller-observer based on the revisited model,

$$\begin{aligned} q_r &= -k_1\hat{u} - k_2\hat{\theta} + \left(k_1 - \frac{f_1 k_2}{g}\right)u_r \\ \dot{\hat{u}} &= -f_1\hat{u} - g\hat{\theta} + l_1(a_x + f_1\hat{u}) \\ \dot{\hat{\theta}} &= g_y + l_2(a_x + f_1\hat{u}), \end{aligned}$$

where u_r is the velocity reference; k_1, k_2 are the controller gains, l_1, l_2 the observer gains. Fig. 5 shows simulation results for the same scenario as before ($1m/s$ reference step in velocity). Two different tunings were used: in the first case ("new design #1") the controller is tuned for a settling time of about $12s$ and the observer for about $48s$, so that the angle and velocity have initial transients similar to the tuning used previously for the usual design (and with a similar control effort); in the second case ("new design #2") the controller is made four times faster.

Both design were successfully implemented, resulting in a quadrotor much easier to fly than with the usual scheme. In practice it was difficult to accelerate much further the time responses, probably mainly because of accelerometer noise.

REFERENCES

[1] P. Castillo, A. Dzul, and R. Lozano, "Real-time stabilization and tracking of a four-rotor mini rotorcraft," *IEEE Transactions on Control Systems Technology*, vol. 12, no. 4, pp. 510–516, 2004.

[2] N. Guenard, T. Hamel, and V. Moreau, "Dynamic modeling and intuitive control strategy for an "X4-flyer"," in *Int. Conf. on Control and Automation*, 2005, pp. 141–146.

[3] F. Kendoul, D. Lara, I. Fantoni-Coichot, and R. Lozano, "Real-time nonlinear embedded control for an autonomous quadrotor helicopter," *Journal of Guidance, Control, and Dynamics*, vol. 30, no. 4, pp. 1049–1061, 2007.

[4] S. Salazar-Cruz, J. Escareño, D. Lara, and R. Lozano, "Embedded control system for a four-rotor UAV," *International Journal of Adaptive Control and Signal Processing*, vol. 21, no. 2-3, pp. 189–204, 2007.

[5] G. Hoffmann, H. Huang, S. Waslander, and C. Tomlin, "Quadrotor helicopter flight dynamics and control: Theory and experiment," in *Collection of Technical Papers - AIAA Guidance, Navigation, and Control Conference 2007*, vol. 2, 2007, pp. 1670–1689.

[6] S. Grzonka, G. Grisetti, and W. Burgard, "Towards a navigation system for autonomous indoor flying," in *IEEE Int. Conf. on Robotics and Automation*, 2009, pp. 2878–2883.

[7] S. Bouabdallah and R. Siegwart, "Full control of a quadrotor," in *IEEE/RSJ Int. Conf. on Intelligent Robots and Systems*, 2007, pp. 153–158.

[8] N. Guenard, T. Hamel, and R. Mahony, "A practical visual servo control for an unmanned aerial vehicle," *IEEE Transactions on Robotics*, vol. 24, no. 2, pp. 331–340, 2008.

[9] F. Kendoul, I. Fantoni, and K. Nonami, "Optic flow-based vision system for autonomous 3d localization and control of small aerial vehicles," *Robotics and Autonomous Systems*, vol. 57, no. 6-7, pp. 591–602, 2009.

[10] M. Achtelik, A. Bachrach, R. He, S. Prentice, and N. Roy, "Stereo vision and laser odometry for autonomous helicopters in GPS-denied indoor environments," in *Proc. SPIE*, vol. 7332, no. 1, 2009, pp. 733 219–10.

[11] P. Pounds, R. Mahony, and P. Corke, "Modelling and control of a quad-rotor robot," in *Australasian Conf. on Robotics and Automation*, 2006.

[12] L. Derafa, T. Madani, and A. Benallegue, "Dynamic modelling and experimental identification of four rotors helicopter parameters," in *IEEE Int. Conf. on Industrial Technology*, 2006, pp. 1834–1839.

[13] T. Madani and A. Benallegue, "Backstepping control with exact 2-sliding mode estimation for a quadrotor unmanned aerial vehicle," in *IEEE/RSJ Int. Conf. on Intelligent Robots and Systems*, 2007, pp. 141–146.

[14] P.-J. Bristeau, P. Martin, E. Salaün, and N. Petit, "The role of propeller aerodynamics in the model of a quadrotor UAV," in *European Control Conf.*, 2009, pp. 683–688.

[15] P. Martin and E. Salaün, "Design and implementation of a low-cost observer-based Attitude and Heading Reference System," *Control Engineering Practice*, pp. –, 2010, in press.

[16] ——, "An invariant observer for Earth-velocity-aided attitude heading reference systems," in *IFAC World Congress*, 2008, paper identifier 10.3182/20080706-5-KR-1001.3577.

[17] P. D. Groves, *Principles of GNSS, inertial, and multisensor integrated navigation systems*. Artech House, 2008.

[18] W. Johnson, *Helicopter Theory*. Princeton University Press, 1980.

[19] P. Kokotovic, H. K. Khalil, and J. O'Reilly, *Singular Perturbation Methods in Control: Analysis and Design*. SIAM, 1999.